Biosensors and Bioelectronics 117 (2018) 567–574

Contents lists available at ScienceDirect

Biosensors and Bioelectronics

journal homepage: www.elsevier.com/locate/bios

Target-triggered three-way junction in conjugation with catalytic concatemers-functionalized nanocomposites provides a highly sensitive colorimetric method for miR-21 detection

Elyas Hosseinzadeh[a], Hadi Ravan[b,*], Abbas Mohammadi[a,*], Rahim Mohammad-rezaei[c], Akram Norouzi[a], Hossein Hosseinzadeh[c]

[a] Department of Clinical Biochemistry, School of Medicine, Kerman University of Medical Sciences, Kerman, Iran
[b] Department of Biology, Faculty of Sciences, Shahid Bahonar University of Kerman, Kerman, Iran
[c] Analytical Chemistry Research Laboratory, Faculty of Sciences, Azarbaijan Shahid Madani University, Tabriz, Iran

ARTICLE INFO

Keywords:
MiR-21
Detection
Colorimetric
Biosensors
MiRNA

ABSTRACT

With the great advances in DNA nanotechnology, scientists have shown interest in developing dynamic nanostructures for theranostic applications, analyte sensing and cargo delivery. Here, we present a specific enzyme-free ultrasensitive platform based on a multilayer coupled signal amplification strategy to quantify miR-21 molecule. The biosensor was integrated based on three signal amplification gadgets, namely a translator-mediated catalytic hairpin assembly (CHA), a multilayer DNA concatemer on the surface of gold decorated magnetic nanoparticle (GMNP), and a DNAzyme-mediated catalytic signal amplification. MiR-21 mediates the release of a DNA translator from an immobilized duplex to engage in a CHA reaction using three hairpins, including a GMNP-conjugated hairpin 1 (H1), biotin-labeled hairpin 2 (H2) and a GMNP-conjugated hairpin 3 (H3) to form a three-way junction (3WJ). Meanwhile, a plenty of initiator strand 0 (S0) on GMNPs – each of which has been bifunctionalized with S0/H1 or S0/H3 – drive several multilayer peroxidase-mimicking DNAzyme concatemers in the presence of two accessory oligonucleotides; strand 1 (S1) and strand 2 (S2). Since a G-rich sequence was attached at the 5′-end of S1 strand, in the presence of hemin cofactor, an active G-quadruplex DNAzyme with peroxidase activity was formed. The concatemers on the surface of GMNPs can convert a colorless substrate to a green product. The biosensor can detect as low as 1 aM of miR-21 and provide an excellent capability to discriminate single-base mismatches. The required time for the formulation of the assay reagents is about three days and the reaction time for the detection of miR-21 takes place in less than four hours.

1. Introduction

Dynamic nucleic acid nanotechnology is built on kinetically controlled DNA strand-displacement reactions, mediated by either enzyme/DNAzyme (Cai et al., 2017; Wickham et al., 2011), chemical-trigger interactions (Wang et al., 2014) or autonomous self-assembly processes (Yin et al., 2008). As a result of their implications for various biomaterial systems, such as information processing (Ravan et al., 2017; Seelig et al., 2006), analyte sensing/signal amplifying (Fozooni et al., 2017; Norouzi et al., 2018; Zhang et al., 2016; Choi et al., 2011; Huang et al., 2014), nanoactuators (Simmel and Yurke, 2001) and cargo delivery (Song et al., 2013), dynamic nanodevices have received considerable attention in recent years. Signal amplification through autonomous DNA self-assembly provides a simple and powerful framework for analyte detection (Zheng et al., 2018) due to the feasibility in design, execution and tuning. Among the most widely used dynamical signal amplification strategies are entropy-driven catalysis (EDC) (D.Y. Zhang et al., 2007), hybridization chain reaction (HCR) (Dirks and Pierce, 2004; Choi et al., 2014) and catalytic hairpin assembly (CHA) (Yin et al., 2008), which tend to exploit kinetically metastable DNA monomers like multi-stranded complexes and hairpins, in order to produce a stable DNA nanostructure. However, coupling the formation of these nanostructures with an appropriate signal transducer has led to the generation of exponential signal amplifications in response to target analytes.

Pioneered by Pierce's group, the autocatalytic target-triggered self-assembly of hairpin monomers through the HCR and CHA technologies has been broadly used within the context of dynamic DNA nanotechnology for signal amplifications. Several research groups have integrated these principal components with different nanomaterials

* Corresponding authors.
E-mail addresses: ravan@uk.ac.ir (H. Ravan), moghabbas@yahoo.com, gh_mohammadi@kmu.ac.ir (A. Mohammadi).

https://doi.org/10.1016/j.bios.2018.06.051
Received 30 March 2018; Received in revised form 22 June 2018; Accepted 26 June 2018
Available online 28 June 2018
0956-5663/

(Huang et al., 2014; Zhao et al., 2017), polymer (Li et al., 2012;), functional nucleic acid (Wang et al., 2011) and enzyme-assisted platforms (Song et al., 2015; Tao et al., 2015) for the analysis of various biomolecules. For instance, Huang et al. (2011), designed a DNA-responsive fluorescent switch based on pyrene excimer formation upon HCR completion. Zhang et al. (2012) developed an improved immuno-HCR assay using bi-functional gold nanoparticles (GNP) and magnetic microparticles in a sandwich format for ultrasensitive detection of human IgG. In a similar strategy, Hau et al. (2015), designed an HCR-based DNAzyme concatemer on GNPs for colorimetric detection of carcinoembryonic antigen. To improve the analytical performance of enzyme-free signal amplification strategies, Wang et al., used CHA and HCR in different studies to induce aggregation of modified GNPs for detection of nucleic acid and adenosine targets (Quan et al., 2015a, 2015b). This group also fabricated hairpin-locked-DNAzyme modified GNPs for detecting miRNA in living cells (Yang et al., 2017). Miao et al. also developed target-stimulated concatemer formation on an electrode-modified DNA tetrahedral nanostructure to detect miRNA molecules (Miao et al., 2015). In another strategy, Ravan designed a modified HCR to construct a multilayer DNAzyme concatemer on GNP for the detection of 16 s rRNA molecules in E. coli bacteria (Ravan, 2016a).

To achieve a powerful biosensing technology with improved sensitivity, specificity and wider dynamic range, a multilayer-integrated signal amplification process needs to be examined. With this in mind, a novel combination of signal amplifiers cached our attention to design an upgrade colorimetric biosensor for the detection of a miRNA with enhanced analytical performance. In this study, we exploited multiple signal amplification strategies to detect miR-21 (Tian et al., 2018) – a short 22-nucleotide RNA molecule which is overexpressed in several human cancers (Wang, 2009; Shah and Calin, 2014) – through the self-assembly of GMNP-labeled oligonucleotides by a CHA reaction. The GMNP-labeled oligonucleotides provide a foundation for the construction of a multilayer G-quadruplex DNAzyme, which in the presence of the hemin molecule produces a colored product. To build this system, two groups of GMNPs were prepared, which were bi-functionalized with hairpin H1/initiator S0 and hairpin H3/S0 (Scheme 1). Hairpin H1 and H3 on different GMNPs formed a catalytic three-way junction self-assembly by recruiting hairpin H2 as the bridge of two GMNPs in the presence of a universal translator as the trigger of the self-assembly process. The single stranded S0 on the GNMPs served as the initiator of the formation of DNA concatemers. The concatemers bore many G-quadraplex domains which produced active DNAzymes with peroxidase activity in the presence of hemin cofactor. In this way, an exponential signal amplification was achieved through (i) the formation of three-way junctions (3WJs), (ii) the formation of multiple DNA concatemers on GMNPs with multilayer G-quadraplex DNAzymes and (iii) the catalytic activity of peroxidase-mimicking DNAzymes to produce a plenty of color products. Through this strategy, attomolar concentrations of the miR-21 can be measured by spectrophotometry.

2. Experimental section

2.1. Materials and reagents

HPLC or PAGE-purified oligonucleotides were synthesized by Bioneer Co. (South Korea), dissolved in deionized water and stored at −20 °C until use. The sequence of oligonucleotides is represented in Table S1. 2, 2′-azino-bis (3-ethylbenzothiazoline-6-sulfonic acid) (ABTS), Tris(2-carboxyethyl) phosphine hydrochloride (TCEP), Hemin, Fe_2O_3, tetrachloroauric (III) acid trihydrate, bovine serum albumin (BSA), streptavidin, dimethyl sulfoxide (DMSO), 4-(2-hydroxyethyl)-1-piperazineethanesulfonic acid (HEPES) and trisodium citrate were purchased from Sigma-Aldrich Co. (USA). Hemin stock solution (0.1 mM) was prepared in DMSO and stored in a dark bottle at −20 °C until required. All aqueous solutions were prepared with deionized water with electrical resistivity of 18.25 (MΩ cm^{-1}). Formation of DNA nanostructure was checked by electrophoresis in a 2.5% agarose gel using 1 × tris-acetate-EDTA buffer at a constant voltage of 80 V for 120 min. The gel was stained by ethidium bromide and visualized using UV-Doc HD 6 light box.

2.2. Preparation and characterization of gold decorated Fe_2O_3 nanocomposites

Gold decorated Fe_2O_3 nanoparticles were synthesized according to Murph's method by using citrate reduction of chloroauric acid (Larsen et al., 2016; Murph et al., 2016). In brief, 100 μL of 25 mM Fe_2O_3 colloid was injected into 10 mL of deionized water under gentle stirring. The mixture was heated for approximately 5 min and 1 mL of 1% citrate solution was added. To the boiling solution, 250 μL of 0.01 M chloroauric acid was added and after 10 min the solution color changed from burnt orange to deep red which proved the formation of Au nanoparticles. The solution was allowed to cool to room temperature and the GMNPs were collected using an external magnet. The separated GMNPs were suspended in deionized water for future use.

2.3. Bi-functionalization of GMNPs with S0/H1 or S0/H3 oligonucleotides

At first, the alkanethiol-caped S0, H1 and H3 oligonucleotides (100 μM) were added to the separate tubes, heated to 95 °C and slowly cooled to room temperature. Then the caped oligonucleotides were converted to active alkanethiol derivatives by adding a solution containing 10 mM TCEP, 10 mM Tris-HCl, 1 mM EDTA and 0.1 M NaCl (pH 7.4). The activated molecules were incubated with GMNPs according to a previously published protocol (J. Zhang et al., 2007). Briefly, 1 mL of GMNPs was incubated with S0/H1 or S0/H3 at different ratios (90:10, 80:20, 70:30, 60:40 and 50:50 with a final concentration of 3 μM) for 16 h at room temperature. To get the maximum loading of the oligonucleotides on GMNPs, salting buffer (10 mM phosphate buffer containing 2.0 M NaCl, pH 7.0) was added dropwise to reach the final salt concentration of 0.1 M NaCl. The mixture was incubated at room temperature for 40 h. Then, the bi-functionalized GMNPs were separated by an external magnet and resuspended in 100 μL of the hybridization buffer (10 mM phosphate buffer supplemented with 200 mM NaCl, 30 mM KCl, and 10 mM $MgCl_2$).

2.4. Colorimetric detection of miR-21

MiRNA-directed signal amplification is limited by its natural features such as vulnerability to degradation and small size (Liao et al., 2015). To overcome these issues, a DNA duplex with translation activity was used (Ravan, 2015). At first, the translator was confined at the surface of microtiter plate wells. For this purpose, each well was incubated with 100 μL of 10 μg/mL streptavidin in RNase-free phosphate buffered saline (PBS) at 4 °C overnight. The wells were then blocked with 250 μL of 1% (w/v) BSA in PBS and then washed out (Ravan and Yazdanparast, 2013, 2012a). To the wells, 100 μL of a biotinylated universal translator – which was pre-formed by heating a mixture of capture and translator oligonucleotides (each 1 μM) to 95 °C and slowly cooled to room temperature – was added and incubated for 30 min.

Different concentrations of miR-21 (80 μL) were added to the wells and incubated for 30 min at room temperature. Based on toehold-mediated DNA strand displacement reaction (TMSD), the translator oligonucleotide is displaced by miR-21 and released in the solution. To the supernatant (70 μL) that contains the translator oligonucleotide, 10 μL biotinylated H2 (1.5 μM), 10 μL H1/S0 bi-functionalized GMNP and 10 μL H3/S0 bi-functionalized GMNP were added and incubated at 25 °C. After 2 h, the GMNPs were settled at the bottom of the tube by a magnet and the solution containing the H2 monomers, which were not used in the 3WJ formation, was discarded. Subsequently, the separated GMNPs were re-suspended in 100 μL hybridization buffer and added to streptavidin-coated wells. After 30 min incubation, the supernatant was

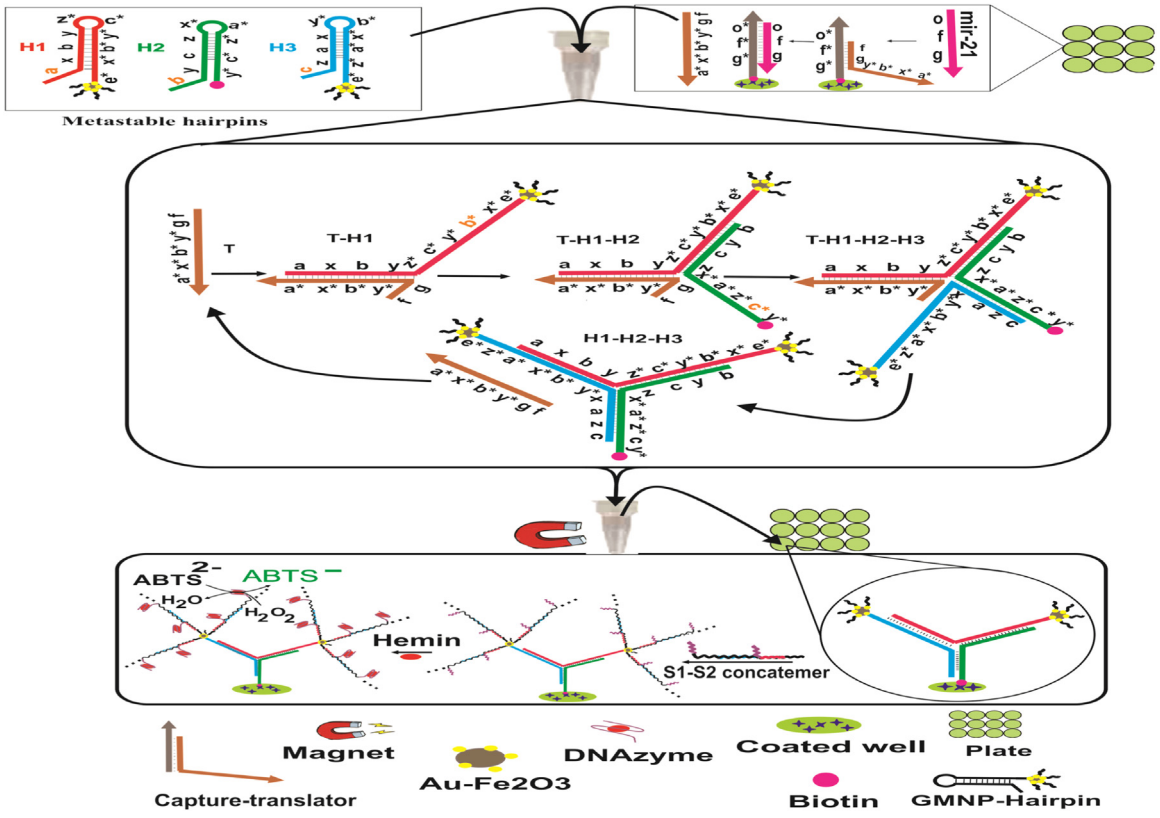

Scheme 1. Catalytic self-assembly of three-way junction. Initially accessible or later exposed toeholds labeled with orange letters trigger assembly reactions. Purple color at the 5′ end of single stranded S1 denotes peroxidase-mimicking DNAzymes.

discarded in order to remove H1/S0 and H3/S0 bi-functionalized GMNPs which did not have biotinylated H2. To each well, 100 μL of 1 μM DNA concatemers, which were pre-formed by heating a mixture of S1 and S2 oligonucleotides (each 1 μM) to 95 °C and slowly cooled to room temperature, was added and incubated for 45 min. After washing, a solution containing 0.5 μM hemin in HEPES buffer (25 mM HEPES, 20 mM KCl, 200 mM NaCl 0.05% Triton X-100% and 1% DMSO) was added to the wells and incubated for 30 min at room temperature (Travascio et al., 1998). To this solution, 100 μL peroxidase substrate (2 mM H_2O_2 and 2 mM ABTS) was added, incubated for 30 min, and the absorbance was measured at 414 nm using the BioTek microtiter plate reader (Ravan, 2016b).

3. Results and discussion

3.1. Design and working principle of dynamical nanodevices

In the present study, we exploited three signal amplification strategies in order to enhance the signal intensity. The first signal amplification layer is mediated by the formation of a plenty of 3WJ structures (conjugated to GMNPs) through the CHA reaction in response to a single DNA translator (released by miR-21). The subsequent layer is mediated by the binding of multiple DNA concatemers to the surface of each GMNP that are triggered by the S0 strands. The last layer is mediated by the peroxidase activity of DNAzymes that resides along each DNA concatemer.

MiRNA-directed signal amplification is limited by its natural properties such as vulnerability to degradation and small size (18–25 nucleotides) (Liao et al., 2015). To overcome these limitations, several strategies have been used including conversion of RNA to complementary DNA, translating RNA to arbitrary DNA (Ravan, 2015), and applying complementary nucleic acid analogues (e.g. peptide nucleic acids (PNAs) and locked nucleic acids (LNAs) (Dong et al., 2011; Jolly et al., 2016)). Among these strategies, the DNA translator can resolve both problems by converting a small and unstable miRNA molecule to a more stable and longer DNA molecule. Moreover, the translators make it possible to detect any analyte by a universal DNA biosensing module. Therefore, translating a miRNA into a universal DNA sequence by the translator can be the best strategy to get a high output signal. Indeed, in the present platform, a TMSD reaction took place by introducing miR-21 and a universal translator was released from the capture-translator duplex. The collected translators were utilized to trigger the formation of 3WJ structure by a series of TMSD reactions.

The three metastable DNA hairpins - GMNP-labeled H1, biotinylated-H2 and GMNP-labeled H3 - in the presence of the universal translator, initiated the formation of 3WJs. This reaction was started by a series of assembly reactions in which the translator was hybridized to the toehold segment “a” of GMNP-labeled H1 and then under a strand displacement reaction, the sequestered segment “b*” is revealed. From the newly exposed segments (x*, b*, y*) that were embedded in the stem region of H1, segment “b* ” serves as a toehold to nucleate to segment “b” of H2 and opens the stem-loop structure of H2. By exposing the ensconcing segments (y*, c*, z*) of H2, the toehold “c*” of H2 invades to H3 and unwinds its stem-loop structure. The reaction proceeds by a disassembly reaction in which the segment “y*” of H3 starts to displace the universal translator and forms a three-way junction (3WJ) nanostructure. The translator molecule now can initiate a new cycle of catalytic hairpin assembly to generate more 3WJ structures. These cascade reactions, however, are kinetically impeded in the absence of a target molecule, because hairpin segments ensconce in stem region of hairpin monomers as stable structures. The subsequent amplification layers are accomplished through S0 strands, which in presence of S1 and S2 strands mediate the formation of multilayer G-quadraplex DNAzyme-concatemers on the surface of GMNPs. The S1 strand contains three functional segments: a 3′-end segment hybridizes to its complementary sequences in S0 and 3′-end of the S2 strand, a middle

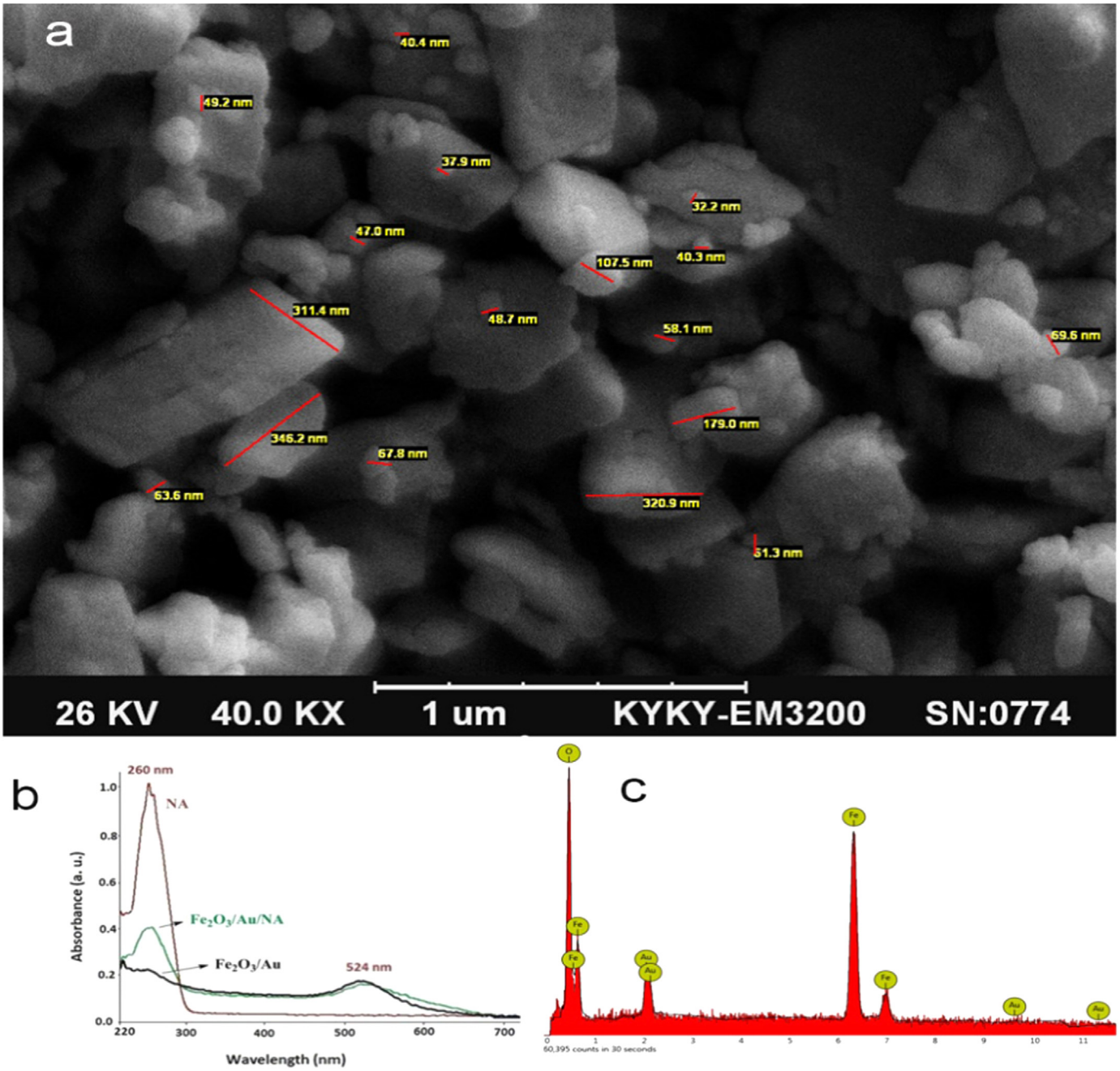

Fig. 1. Characterization of GMNP nanocomposite. (a) Morphology analyses of synthesized GMNPs using SEM with the average diameters of 250 nm, (b) UV–vis spectra of purified nucleic acid, GMNP and oligonucleotide-functionalized GMNP, (c) EDX spectrum of the GMNPs.

segment is complementary to 5′-end of S2 and a 5′-end G-rich sequence that in the presence of hemin is configured to form an active peroxidase-mimicking DNAzyme. The active DNAzymes are, in the presence of hydrogen peroxide, capable of converting colorless 2,2′-azino-bis(3-ethylbenzothiazoline-6-sulfonic acid) ($ABTS^{2-}$) to the greenish $ABTS^{\bullet-}$ which could be measured at the 414 nm.

3.2. Characterization of gold decorated Fe_2O_3 nanoparticles

Hybrid nanocomposites were analyzed with SEM to examine the morphology of the Fe_2O_3-Au nanoparticles. Irregular particles with smaller rounded particles on their surfaces (Fig. 1a) appeared to be Fe_2O_3 nanoparticles which were decorated with Au nanoparticles with 30–50 nm diameters. The UV–vis spectrum shows the peak absorbance at 525 nm corresponding to Au nanoparticles (Murph et al., 2016). Since the similar peak is observed in Fe_2O_3-Au hybrid nanocomposite samples (after purification of the decorated nanocomposites), the Au-Fe_2O_3 hybrid structure formation is confirmed. Besides, observation of peak intensity at 260 nm, corresponding to nucleic acid absorbance, confirmed successive functionalization of GMNPs with DNA oligonucleotides as seen in Fig. 1b (Kashanian et al., 2012). Furthermore, Fig. 1c depicts EDX spectrum of synthesized Fe_2O_3-Au nanocomposite as an indicator of elements of interest, confirming the presence of O, Fe and Au in the sample. According to this analysis, presence of ferric oxide and Au was observed on the synthesized nanocomposite.

3.3. Confirmation of 3WJ construction by gel electrophoresis

To analyze the CHA performance in the formation of 3WJ, agarose gel electrophoresis was used. As indicated in Fig. 2, two bands

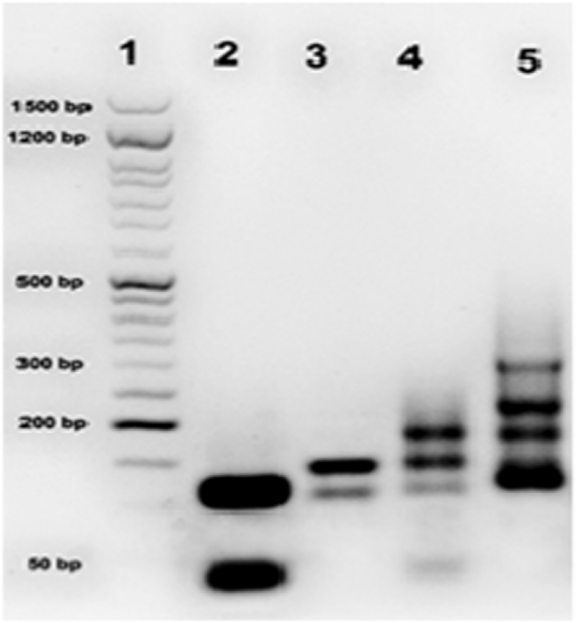

Fig. 2. Confirmation of CHA reaction and formation of 3WJ by 2.5% agarose gel electrophoresis. Lane 1; DNA marker, lane 2 (H1 + H2 + H3); lane 3 (T + H1); lane 4 (T + H1 + H2); lane 5 (T + H1 + H2 + H3).

corresponding to H1 and H3 (upper band) and H2 (lower band) were observed (lane 2), suggesting that in the absence of the translator (released by mir-21), the monomers could not assemble to form the 3WJ structure. In contrast, three different intensive bands with obvious shift in the positions, compared to the control sample (lane 2), were seen around 150–300 bp in the presence of the translator (lane 5), which shows that the translator accelerates the assembly and disassembly reactions and most of the hairpins are consumed for the construction of the expected 3WJ structures. Observing several bands in lane 5 encouraged us to explore the source of these bands by incubating the translator with H1 (lane 3) and H1/H2 (lane 4) monomers. In contrast to control sample (lane 2), different bands were obtained in lanes 3 and 4, corresponding to translator-accelerated monomers assembly, which represent the sequential monomer consumption by the CHA reaction. In this respect, in lane 5, the upper-most band is a quaternary complex of T-H1-H2-H3, the middle band represents a ternary complex of H1-H2-H3 and the lower one is related to the T-H1-H2 complex. These results suggest that the multiple bands observed in the test sample (lane 5) result from the formation of different complexes in the presence of the translator molecule (T-H1-H2, H1-H2-H3 [the product] and T-H1-H2-H3).

3.4. Optimization of the System Variables

To achieve the best sensing performance, different experimental parameters including the ratio of initiator to hairpin monomers on GMNPs, temperature and time for the CHA-3WJ reaction and hemin concentration for the DNAzyme activity were optimized. Initially, to maximize the sensitivity of the assay, the ratio of initiator to hairpin monomers on the GMNP surface was optimized. Theoretically, the highest signal is obtained on the condition that GMNP is loaded with maximal S0 and minimal hairpin concentrations. On this basis, we used different concentrations of S0 and hairpin monomers (H1 or H3) at a ratio of (50:50, 60:40, 70:30, 80:20, 90:10) at a final concentration of 3 μM. Since in the present study we used a pre-formed and fixed-concentration of S1-S2 concatemer, the signal intensity was solely dependent on the ratio of S0 to H1 and H3. As shown in Fig. 3a, the maximum signal intensity was obtained at a ratio of 60:40 (S0 to H1 or H3) corresponding to the S0 concentration of 1.8 μM and declined at higher concentrations of S0 (2.1–2.7 μM). Enhancement of the signal intensity in a concentration-dependent manner by increasing the S0 level is due to the sufficient loading of S0 on the GMNPs. However, decreasing the signal intensity at higher concentrations of S0 is explained by insufficient loading of hairpins (H1/H3) on the GMNPs surfaces. Our result is in agreement with the previous finding that the optimum ratio of oligonucleotides for bifunctionalized AuNP-based assays was found to be 60:40–70:30 (Ravan, 2016a).

The formation of stable 3WJs is dependent on the experiment conditions, such as salt concentration, temperature and duration of the reaction. All parameters are associated with thermodynamic issues in which kinetically hindered duplexes could be opened by initiators to form more stable nanostructures. As seen in Fig. 3b, the optimum incubation time was 2 h. At time intervals higher than 2 h, the ratio of signal to background is gradually diminished that in turn compromises the assay sensitivity by increasing nonspecific interactions between hairpins. The assay efficiency at different temperatures between 10 and 35 °C was also optimized. As shown in Fig. 3c, the highest signal to background ratio was gained at 25 °C and at higher temperatures a decrease in the signal intensity was observed due to system leak.

It has been well demonstrated that endogenous or SELEX-based fabricated G-rich DNAzymes show peroxidase mimicking activity in the presence of hemin. On the other hand, the peroxidase activity of hemin is intensively increased by binding to G-quadraplex sequence. Due to their easy synthesis, manipulation, stability and small size, several G-quadruplex-hemin DNAzymes have been selected as a signal transducer in biosensors, biomaterials and biomolecular devices. Taken the reaction efficiency into account, a series of hemin samples at concentrations ranging from 0.25 to 1 μM were applied to induce the maximum signal output. As seen in Fig. 3d, the signal to noise (S/N) reaches the maximum level at 0.5 μM hemin and at higher concentrations the S/N ratio reaches to the plateau phase because of high background despite of high sample absorbance.

3.5. Analytical performance of the nanodevice

To identify the analytical performance of the assay, its ability to respond to certain target concentrations was examined. Fig. 4 displays the spectral data collected for various target concentrations under the optimum conditions in the range of 1 aM to 7.5 pM As shown, with the increase of concentration from 1 aM to 5 pM, the absorbance also increased and reached to plateau in higher concentrations. Limit of detection (LOD) of the assay was 1 aM based on 3σ rule (the threshold value is 0.16). Moreover, the assay exhibited excellent linearity between the logarithm of the miR-21 input and the absorbance values over 6 orders of magnitude (1 aM to 5 pM) with a correlation coefficient of 0.98 ($Abs = 0.0838 \log C + 0.1905$). To our knowledge, in the preliminary coupled CHA-HCR approach pioneered by Ellington group (Jiang et al., 2012), each CHA reaction provides a single initiation site for the HCR reaction and consequently each CHA event feeds a single HCR reaction. However, in the present approach, the signal amplification is improved by GMNP-conjugated CHA-3WJ whereby each nanoparticle is loaded with hundreds of initiation sites through its S0-modified surface and might execute hundreds of modified HCR. It is worthy to point out that we also evaluated single probe (H1) labeling with GMNP, but the signal was clearly lower than the both probe labeling (Supplementary information, Fig. S1). Besides, we applied an external magnetic field and then streptavidin-coated surfaces to remove non-reacted H2 monomers, excessive bi-functionalized GMNPs and translators. Since the S0 strands may adversely affect the attachment of hairpin monomers to GMNPs, we added an oligo sequence as a spacer for hairpin monomers to easily attach to GMNP surfaces without any steric hindrance.

As a broadly used methodology for amplifying low-abundance nucleic acids and validating results from screening experiments, RT-qPCR amplification can be considered as a gold standard method for miRNA

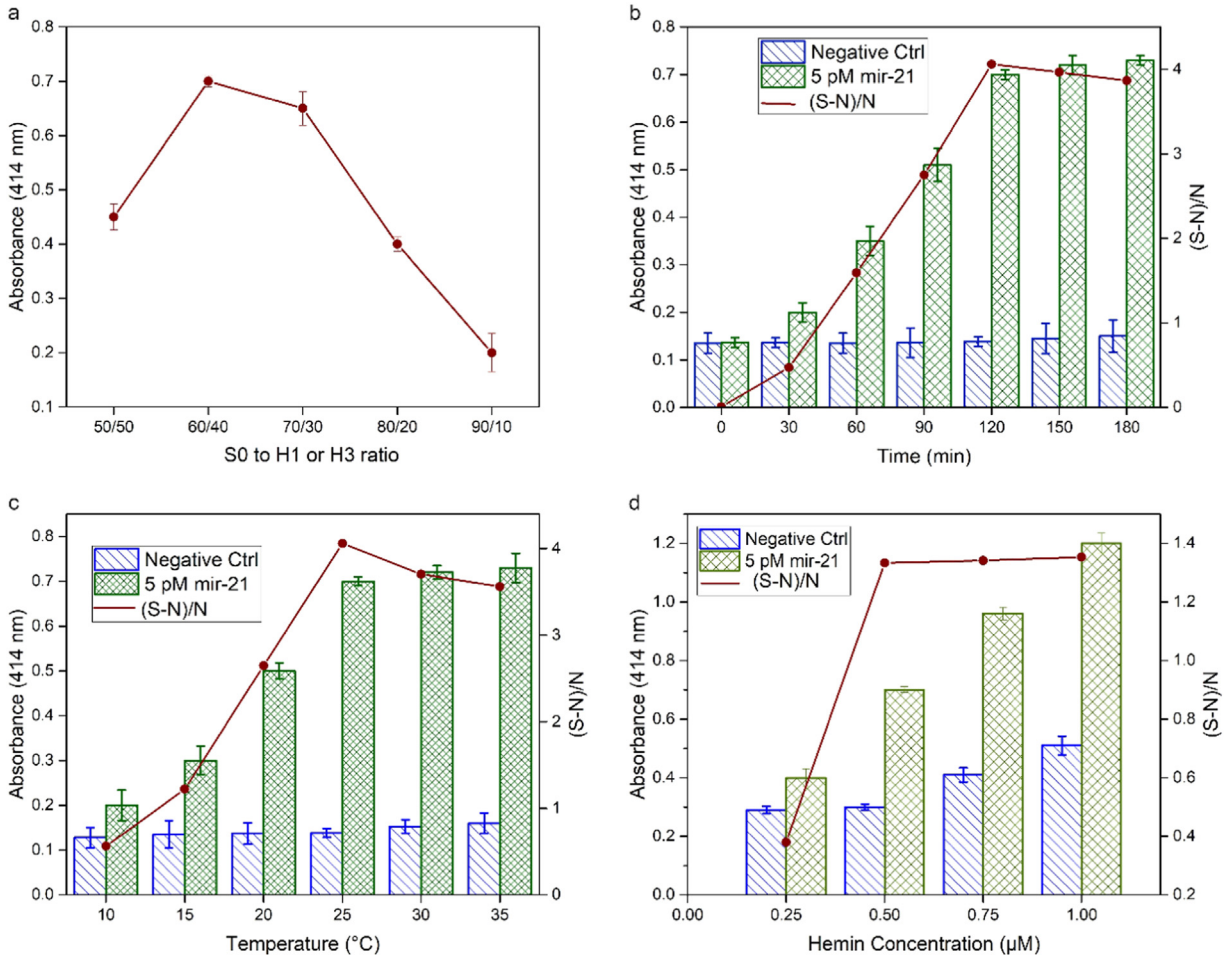

Fig. 3. Optimization of assay conditions for colorimetric detection of miR-21. (a) Concentration of S0 to H1/H3 ratio for GMNPs bi-functionalization. (b) Optimum incubation time and (c) temperature needed for CHA-3WJ formation. (d) Optimum hemin concentration for maximum DNAzyme activation. Error bars represent standard deviations from three repeated experiments.

detection. This technique, however, suffers from certain technical challenges such as infeasibility for in situ and intracellular applications, enzyme inactivation and requirement for large and expensive thermal cyclers which limit its application in resource-limited settings and for point-of-care (POC) analysis (Androvic et al., 2017; Chen et al., 2005; Bi et al., 2017). In contrast, isothermal amplification methods (Ravan et al., 2016; Ravan and Amandadi, 2015; Ravan and Yazdanparast, 2012b), in particular, enzyme-free isothermal signal amplification can entirely overcome the drawbacks of enzymatic and thermocycler dependent methods. Indeed, numerous studies have addressed the use of isothermal enzyme-free signal amplification to develop ultrasensitive biosensors for miRNA detection (Liu et al., 2015; Zhang et al., 2016; Zhang et al., 2017). An inspiring fact is that, in terms of the limit of detection and portability, the present DNA nanodevice is superior to a

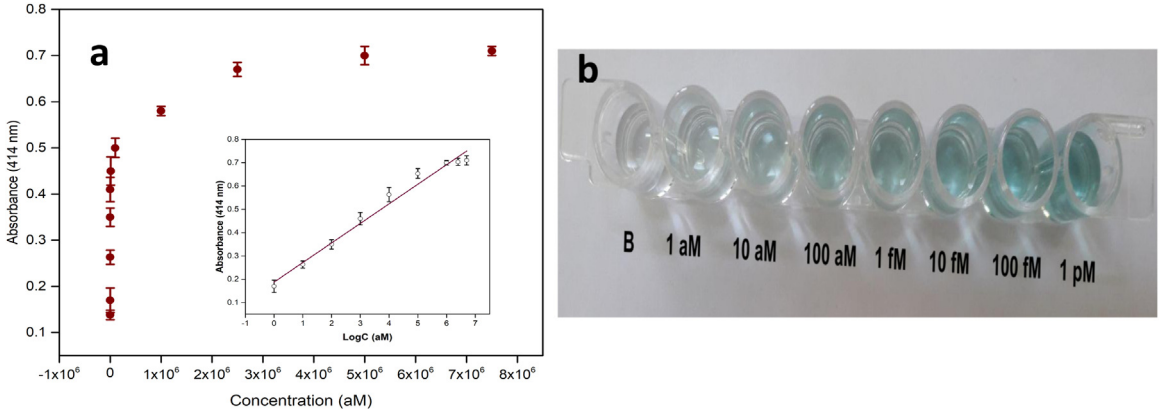

Fig. 4. Analytical performance of the assay. a) Calibration curve obtained from the absorbance values at 414 nm. Inset showed linear plot of the absorbance intensity vs. logarithmic concentration of miR-21 over the range of 1 aM to 8 pM b) Corresponding catalytic coloring results ranging from 1 aM to 1 pM B, indicted as blank. Error bars show the standard deviations of triplex experiments.

Table 1
Comparative analyses of DNA nanodevice and previous assays for nucleic acid detection based on isothermal signal amplification.

Reference	Limit of detection	Single base mismatch specificity (SBS)[a]
Yang et al. (2012)	1 pM	20–35%
Qing et al. (2014)	10 pM	19–49%
Liu et al. (2015)	0.5 pM	~ 39%
Xing et al. (2017)	1.5 pM	~34%
Harcourt and Kool (2012)	200 pM	65%
Current study	1 aM	20–25%

[a] Supplementary information.

considerable number of isothermal enzyme-free and even enzyme-based strategies (Table 1).

Despite the impressive progress made in the development of enzyme free systems, the assay reaction time and its complexity are the challenges, which need to be improved to meet the demand for simple and rapid detection of nucleic acids. Some strategies could be employed to decrease reaction time of assay which in turn makes the assay less complex. For example, merging of translator releasing step, CHA-3WJ performing step and concatemer immobilization step, minimize the washing steps and save the assay reaction time about 90 min, just with precise designing and a little optimization.

3.6. Analyzing the specificity of the nanodevice

Polymorphism and mutation are genetic variations arising from unrepaired DNA errors such as addition, deletion or substitution of one or more nucleotides that can alter the whole structure of a chromosome. Ability to sense these variations is of great importance to sense-and-treat individuals based on genetic variations in personalized medicine procedure (Scott et al., 2012; Stenson et al., 2009). To precisely evaluate the specificity of the nanodevice in discriminating of single-nucleotide mutation, three synthetic target molecules, each with a single nucleotide mutation in the same position under identical conditions, were used. Depicted in Fig. 5a, the target molecule (miR-21) induces obvious signals in comparison to other analogues. Although a slight increase in the signal intensity was observed in the presence of 5 pM substituted analogue, it is not comparable with when 5 pM perfect the target (miR-21) is present. In recent years, several strategies based on CHA-3WJ have been developed for nucleic acids detection by single nucleotide polymorphism discrimination ability. Spatially sensitive pyrene excimer switching to generate fluorescent signal through CHA-3WJ were used to detect a target nucleic acid (Qing et al., 2014). In another study, Liu et al., developed an electrochemical based CHA mediated 3WJ formation on the electrode surface for detecting nucleic acids (Liu et al., 2015). Moreover, Xing et al., developed CHA-3WJ based method to elucidate miRNA by surface plasmon resonance (SPR) technique (Xing et al., 2017). In comparison, the present nanodevice provides a higher specificity than the aforementioned methods and also it is a desirable method for reliable detection of nucleic acids (Table 1).

3.7. Application of the nanodevice for the detection of miR-21 in real sample

To confirm the generality and feasibility of the proposed assay for analyzing target molecules in real samples, miR-21 was spiked into human serum to mimic the same environment with real samples (Huang et al., 2014; Zhou et al., 2014). In this respect, the serum samples were initially diluted 10 times with 0.1 M PBS (pH 6.0) and were then spiked with three miR-21 concentrations (0.1, 10, 1000 fM), then the signal was recorded (Fig. 5b). Absorption intensity at 414 nm that was obtained from the diluted serum samples revealed no significant difference compared to those in buffer solutions. Like in buffer, the presence of 0.1 fM miR-21 in the diluted human serum can be differentiated from the blank samples that indicate the feasibility of the present approach for visual detection of the miR-21 in real physiological conditions.

4. Conclusion

In summary, using GMNP-labeled CHA-3WJ as a foundation for multiple catalytic nanowires, a novel multi-coupled signal amplifier was illustrated in the present study. This dynamic DNA nanodevice possesses four distinctive characteristics: i) The GMNP-labeled hairpins involved in the CHA-3WJ reaction serve as a foundation for the formation of multiple DNAzyme-modified concatemers. The DNAzymes can convert a colorless substrate to a greenish compound, providing ultra-signal amplification; ii) This nanodevice recruits miR-21-released translator as a fuel for CHA-3WJ construction and S0 strand on GMNP for multi-layer DNAzyme formation, while background signal is totally circumvented by consecutive purification; iii) The assay easily discriminates a single mismatch due to the stringently designed amplification pathway, providing a highly specific method; iv) This method has a practical usability to interrogate clinical samples. In such a

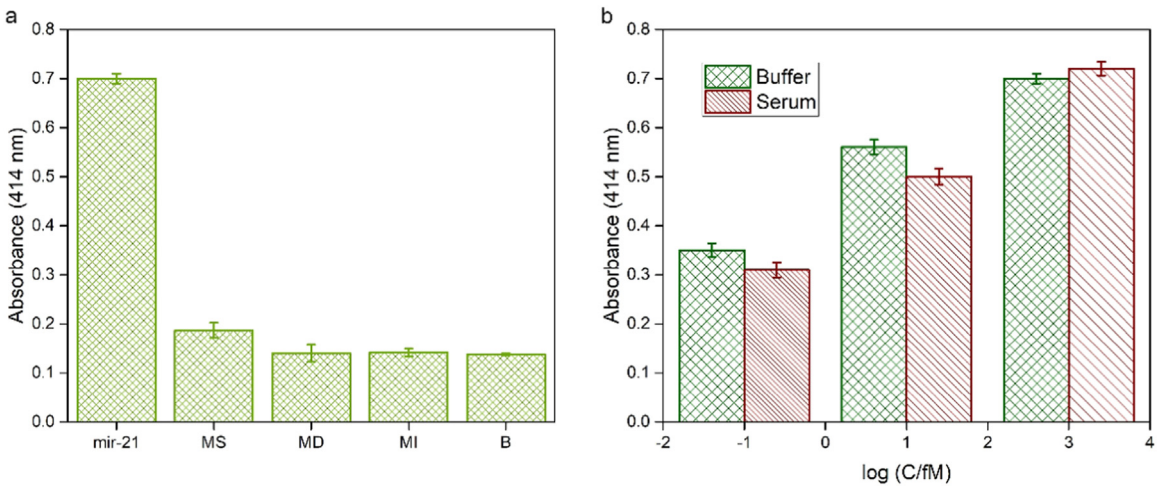

Fig. 5. a) Assay specificity of the DNA nanodevice toward 5 pM miR-21. MS, MD and MI are synthetic miR-21 molecules with single nucleotide substitution, deletion and insertion in identical position, respectively and B represents the blank. b) Comparative data on the signal obtained by log concentration of different mir-21 inputs (0.1, 10, 1000 fM) in buffer and diluted serum sample. The error bars represent standard deviations of triplex measurements.

condition, the proposed dynamic DNA nanodevice is a progressive achievement in material science, drug delivery, nano-biomedicine and biosensing, offering feasible routes toward achieving versatile and powerful molecular machines.

Acknowledgments

This work was supported by Kerman University of Medical Science, Kerman, Iran (grant number 95.177).

Appendix A. Supporting information

Supplementary data associated with this article can be found in the online version at http://dx.doi.org/10.1016/j.bios.2018.06.051.

References

Androvic, P., Valihrach, L., Elling, J., Sjoback, R., Kubista, M., 2017. Nucleic Acids Res. 45, e144.
Bi, S., Yue, S., Zhang, S., 2017. Chem. Soc. Rev. 46, 4281–4298.
Cai, W., Xie, S., Zhang, J., Tang, D., Tang, Y., 2017. Biosens. Bioelectron. 98, 466–472.
Chen, C., Ridzon, D.A., Broomer, A.J., Zhou, Z., Lee, D.H., Nguyen, J.T., Barbisin, M., Xu, N.L., Mahuvakar, V.R., Andersen, M.R., 2005. Nucleic Acids Res. 33 (e179–e179).
Choi, H.M., Beck, V.A., Pierce, N.A., 2014. ACS Nano 8, 4284–4294.
Choi, J., Love, K.R., Gong, Y., Gierahn, T.M., Love, J.C., 2011. Anal. Chem. 83, 6890–6895.
Dirks, R.M., Pierce, N.A., 2004. Proc. Natl. Acad. Sci. USA 101, 15275–15278.
Dong, H., Ding, L., Yan, F., Ji, H., Ju, H., 2011. Biomaterials 32, 3875–3882.
Fozooni, T., Ravan, H., Sasan, H., 2017. Appl. Biochem. Biotechnol. 183, 1224–1253.
Harcourt, E.M., Kool, E.T., 2012. Nucleic Acids Res. 40, e65.
Hou, L., Wu, X., Chen, G., Yang, H., Lu, M., Tang, D., 2015. Biosens. Bioelectron. 68, 487–493.
Huang, J., Gao, X., Jia, J., Kim, J.-K., Li, Z., 2014. Anal. Chem. 86, 3209–3215.
Huang, J., Wu, Y., Chen, Y., Zhu, Z., Yang, X., Yang, C.J., Wang, K., Tan, W., 2011. Angew. Chem. Int. Ed. 50, 401–404.
Jiang, Y., Li, B., Chen, X., Ellington, A.D., 2012. Molecules 17, 13211–13220.
Jolly, P., Batistuti, M.R., Miodek, A., Zhurauski, P., Mulato, M., Lindsay, M.A., Estrela, P., 2016. Sci. Rep. 6, 36719.
Kashanian, S., Rafipour, R., Tarighat, F.A., Ravan, H., 2012. IET Nanobiotechnol. 6, 102–109.
Larsen, G.K., Farr, W., Hunyadi Murph, S.E., 2016. J. Phys. Chem. C. 120, 15162–15172.
Li, B., Chen, X., Ellington, A.D., 2012. Anal. Chem. 84, 8371–8377.
Liao, Y., Fu, Y., Wu, Y., Huang, R., Zhou, X., Xing, D., 2015. Biomacromolecules 16, 3543–3551.
Liu, S., Wei, W., Liu, T., Wang, L., 2015. Chem. Asian J. 10, 1903–1908.
Miao, P., Tang, Y., Zhang, Q., Bo, B., Wang, J., 2015. Chempluschem 80, 1712–1715.
Murph, S.E.H., Larsen, G.K., Lascola, R.J., 2016. JoVE (J. Vis. Exp.) (e53598–e53598).
Norouzi, A., Ravan, H., Mohammadi, A., Hosseinzadeh, E., Norouzi, M., Fozooni, T., 2018. Anal. Chim. Acta 1017, 26–33.
Qing, Z., He, X., Huang, J., Wang, K., Zou, Z., Qing, T., Mao, Z., Shi, H., He, D., 2014. Anal. Chem. 86, 4934–4939.
Quan, K., Huang, J., Yang, X., Yang, Y., Ying, L., Wang, H., He, Y., Wang, K., 2015a. Chem. Commun. 51, 937–940.
Quan, K., Huang, J., Yang, X., Yang, Y., Ying, L., Wang, H., Wang, K., 2015b. Analyst 140, 1004–1007.
Ravan, H., 2016a. Biosens. Bioelectron. 80, 67–73.
Ravan, H., 2016b. Anal. Chim. Acta 910, 68–74.
Ravan, H., 2015. TrAC Trends Anal. Chem. 65, 97–106.
Ravan, H., Amandadi, M., 2015. Curr. Microbiol. 71, 274–282.
Ravan, H., Amandadi, M., Esmaeili-Mahani, S., 2017. Anal. Chem. 89, 6021–6028.
Ravan, H., Amandadi, M., Sanadgol, N., 2016. Microb. Pathog. 91, 161–165.
Ravan, H., Yazdanparast, R., 2013. Anal. Biochem. 439, 102–108.
Ravan, H., Yazdanparast, R., 2012a. Anal. Chim. Acta 733, 64–70.
Ravan, H., Yazdanparast, R., 2012b. World J. Microbiol. Biotechnol. 28, 2101–2106.
Scott, C.T., Caulfield, T., Borgelt, E., Illes, J., 2012. Nat. Biotechnol. 30, 141.
Seelig, G., Soloveichik, D., Zhang, D.Y., Winfree, E., 2006. Science 314, 1585–1588.
Shah, M.Y., Calin, G.A., 2014. Wiley Interdiscip. Rev. RNA 5, 537–548.
Simmel, F.C., Yurke, B., 2001. Phys. Rev. E 63, 41913.
Song, C., Wang, Z., Ding, B., 2013. Small 9, 2382–2392.
Song, W., Zhang, Q., Sun, W., 2015. Chem. Commun. 51, 2392–2395.
Stenson, P.D., Mort, M., Ball, E.V., Howells, K., Phillips, A.D., Thomas, N.S.T., Cooper, D.N., 2009. Genome Med. 1, 13.
Tao, C., Yan, Y., Xiang, H., Zhu, D., Cheng, W., Ju, H., Ding, S., 2015. Chem. Commun. 51, 4220–4222.
Tian, L., Qian, K., Qi, J., Liu, Q., Yao, C., Song, W., Wang, Y., 2018. Biosens. Bioelectron. 99, 564–570.
Travascio, P., Li, Y., Sen, D., 1998. Chem. Biol. 5, 505–517.
Wang, F., Elbaz, J., Orbach, R., Magen, N., Willner, I., 2011. J. Am. Chem. Soc. 133, 17149–17151.
Wang, F., Lu, C.-H., Willner, I., 2014. Chem. Rev. 114, 2881–2941.
Wang, X., 2009. RNA 15, 716–723.
Wickham, S.F.J., Endo, M., Katsuda, Y., Hidaka, K., Bath, J., Sugiyama, H., Turberfield, A. J., 2011. 6, 166–169.
Xing, Y., Li, X., Yuan, T., Cheng, W., Li, D., Yu, T., Ding, X., Ding, S., 2017. Analyst 142, 4834–4842.
Yang, L., Liu, C., Ren, W., Li, Z., 2012. ACS Appl. Mater. Interfaces 4, 6450–6453.
Yang, Y., Huang, J., Yang, X., He, X., Quan, K., Xie, N., Ou, M., Wang, K., 2017. Anal. Chem. 89, 5850–5856.
Yin, P., Choi, H.M.T., Calvert, C.R., Pierce, N.A., 2008. Nature 451, 318–322.
Zhang, B., Liu, B., Tang, D., Niessner, R., Chen, G., Knopp, D., 2012. Anal. Chem. 84, 5392–5399.
Zhang, D.Y., Turberfield, A.J., Yurke, B., Winfree, E., 2007. Science 318, 1121–1125.
Zhang, H., Wang, Q., Yang, X., Wang, K., Li, Q., Li, Z., Gao, L., Nie, W., Zheng, Y., 2017. Analyst 142, 389–396.
Zhang, J., Song, S., Wang, L., Pan, D., Fan, C., 2007. Nat. Protoc. 2, 2888–2895.
Zhang, Y., Gao, D., Fan, J., Nie, J., Le, S., Zhu, W., Yang, J., Li, J., 2016. Biosens. Bioelectron. 78, 538–546.
Zhao, J., Jing, P., Xue, S., Xu, W., 2017. Biosens. Bioelectron. 87, 157–163.
Zheng, W., Yao, L., Teng, J., Yan, C., Qin, P., Liu, G., 2018. Sens. Actuators B Chem. 264, 320–326.
Zhou, W., Gong, X., Xiang, Y., Yuan, R., Chai, Y., 2014. Biosens. Bioelectron. 55, 220–224.